Quantum interference effects in antidot lattices in magnetic fields

Takeshi Nakanishi and Tsuneya Ando

Institute for Solid State Physics, University of Tokyo, 7-22-1 Roppongi, Minato-ku, Tokyo 106, Japan

A numerical study is performed on quantum interference effects in antidot lattices in a weak magnetic field with the use of a recursive Green's function technique. An irregular Aharonov-Bohm (AB)-type oscillation varying sensitively with antidot diameters and periods is dominant in ideal antidot lattices. The AB-type oscillation disappears and an Al'tshuler, Aranov, and Spivak (AAS) oscillation manifests itself in the presence of fluctuations in the size or position of antidots. The AAS oscillation is much stronger in hexagonal lattices than in square lattices, in good agreement with experiments. [S0163-1829(96)08335-X]

I. INTRODUCTION

Recent developments in crystal growth and microfabrication technology have made it possible to obtain ballistic electrons controlled by using artificial structures. A two-dimensional (2D) electron system with a lattice of a depleted circular region called an antidot has been realized in a high-mobility $GaAs/Al_xGa_{1-x}As$ heterostructure. Such systems are usually called antidot lattices. The purpose of the present paper is to study quantum-interference effects on the transport in such antidot lattices.

During the past several years, magnetoresistance in antidot lattices has attracted considerable attention. In antidot lattices, the elastic and inelastic scattering lengths (~ 10 μm, typically) are usually much longer than the lattice period ($\gtrsim 200$ nm, typically). The diagonal resistivity exhibits distinct peaks when the classical cyclotron orbit fits around a certain number of antidots.[1-3] This commensurate oscillation can be understood in classical mechanics.[4]

On the other hand, measurements at very low temperatures revealed quantum oscillations. A fine structure[5,6] is superimposed upon the commensurate peak, which is explained by the semiclassical quantization of periodic orbits existing in the chaotic electron motion.[5,7,8] Recently, an Al'tshuler, Aronov, and Spivak (AAS) oscillation[9] was observed in antidot lattices with small lattice periods (~ 200 nm).[10-12]

The Aharonov-Bohm (AB) and AAS oscillations of the conductance have been known as typical quantum-interference effects caused by the AB effect.[13] The AAS oscillation was observed in a conductor having the form of a hollow cylinder, and characterized by the oscillation as a function of the magnetic flux passing through its cross section with period given by a half of the flux quantum $\phi_0 = ch/e$.[14] It was also observed experimentally[15] and analyzed theoretically[16] in networks of thin metallic wires. Usually, the AAS oscillation is characteristic of diffusive systems, where the mean free path is much smaller than the size of typical geometric structures.

The AAS oscillation appears in the conductance averaged over many different samples, and therefore does not require the whole system to be coherent. On the contrary, the AB oscillation characterized by the ϕ_0 period requires coherence in the whole system, because it has a phase varying from system to system and cancels out completely after the average over many different systems. The AB oscillation was also observed in a ballistic ring made of a high-mobility 2D system,[17] and was theoretically analyzed.[18]

In this paper, we calculate the conductance of antidot lattices with a finite size and discuss under which conditions AAS oscillations become observable. In Sec. II, the model and the procedure of the calculation are described. In Sec. III, the conductance is calculated as a function of a magnetic field, and the dependence on the strength of impurity scattering, fluctuations in the antidot, and the lattice structure are discussed. Discussions and conclusions are given in Sec. IV. A preliminary account of a part of this work was presented.[19]

There have been various theoretical investigations of magnetotransport in antidot lattices in which quantum-interference effects are taken into account.[20-27] Some such works studied dot or antidot arrays in high magnetic fields where edge states play an important role.[20-24] Some considered only a system having a lattice period much smaller than that in realistic antidots.[25,27] In the present calculation, both the lattice period and antidot potential are chosen in such a way that the model simulates actual systems quite well.[10-12]

II. MODEL AND METHOD

In order to study interference effects in antidot lattices, we shall consider systems having a finite size and containing a finite number of antidots. The potential of an antidot in a Wigner-Seitz cell is given by

$$v_{\mathbf{R}}(\mathbf{r}) = U_0(\mathbf{R})F(\mathbf{r}-\mathbf{R}), \qquad (2.1)$$

where $U_0(\mathbf{R})$ is the maximum potential height for the cell specified by lattice point $\mathbf{R}$. The lattice point is written as $\mathbf{R} = n_1\mathbf{a}_1 + n_2\mathbf{a}_2$ with integers n_1 and n_2, where $\mathbf{a}_1$ and $\mathbf{a}_2$ are the primitive translation vectors.

For a hexagonal antidot lattice with lattice constant a, we have $\mathbf{a}_1 = (\sqrt{3}/2, \frac{1}{2})a$ and $\mathbf{a}_2 = (0,1)a$. The potential of each antidot is chosen as

$$F(\mathbf{r}) = \left| \cos\left(\frac{\pi\mathbf{a}_1\cdot\mathbf{r}}{a^2}\right)\cos\left(\frac{\pi\mathbf{a}_2\cdot\mathbf{r}}{a^2}\right)\cos\left(\frac{\pi(\mathbf{a}_1-\mathbf{a}_2)\cdot\mathbf{r}}{a^2}\right) \right|^{4\beta/3}, \qquad (2.2)$$
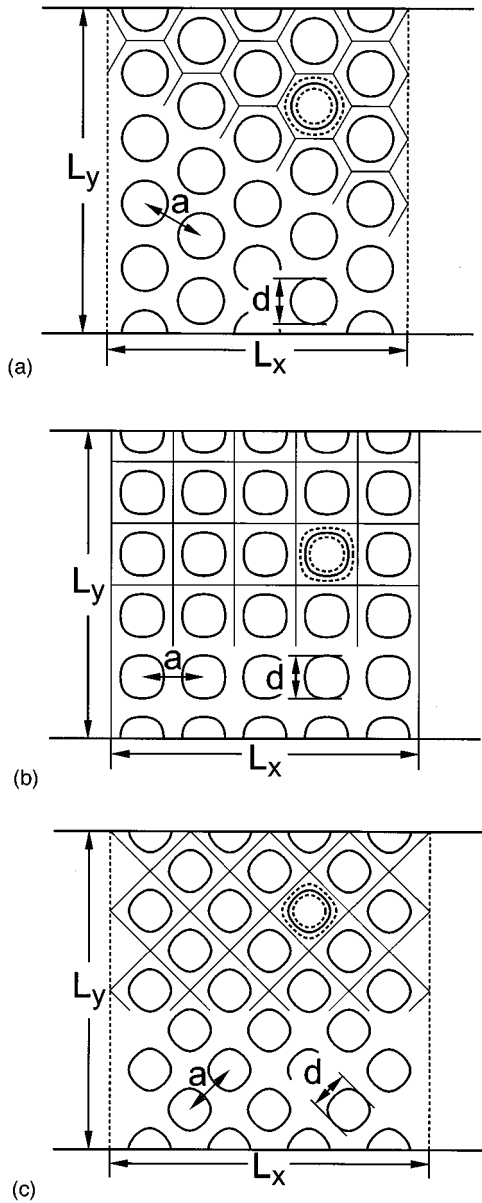
FIG. 1. A schematic view of the cross section of the antidot potential at the Fermi energy for finite-size antidot lattice. The system is connected to an ideal wire or lead in the x direction and confined by an abrupt and infinite barrier in the y direction. The dotted lines denote contour lines of the antidot potential at $v_R(\mathbf{r})/E_F = 0.25$ and 2, and the thin solid lines are boundaries of Wigner-Seitz cells. (a) Hexagonal lattice. (b) Square lattice with a primitive translation vector parallel or perpendicular to the direction of the current. (c) Square lattice with a primitive translation vector inclined 45° from the direction of the current.

where β is a parameter describing the steepness of the potential. For a square lattice with lattice constant a, on the other hand, we use[4]

$$F(\mathbf{r}) = \left| \cos\left(\frac{\pi x}{a}\right) \cos\left(\frac{\pi y}{a}\right) \right|^{2\beta}, \qquad (2.3)$$

and $\mathbf{a}_1 = (1,0)a$ and $\mathbf{a}_2 = (0,1)a$. An antidot diameter d_R is defined as $d_R = |\mathbf{r} - \mathbf{R}|$, with $v_R(\mathbf{r}) = E_F$, where E_F is the Fermi energy and $\mathbf{r}$ is chosen on a line connecting $\mathbf{R}$ and one

of its nearest-neighbor points (e.g., $\mathbf{R} + \mathbf{a}_1$). In the above the exponents, $4\beta/3$ and 2β in Eqs. (2.2) and (2.3), respectively, have been chosen in such a way that the total exponent of the cosine function becomes 4β, for which the potential maximum U_0 and the gradient at the Fermi energy are about the same in the hexagonal and triangular lattices for antidot diameters $d/a = 0.6 \sim 0.7$ and steepness $\beta = 1 \sim 2$.

We shall calculate the conductance of a system with a rectangular form with length L_x and width L_y, connected to an ideal wire in the x direction and confined by an abrupt and infinite barrier in the y direction. We shall replace the 2D system by a rectangular lattice with lattice constants a_x and a_y and nearest-neighbor transfer integrals t_x and t_y. We set $a_x = (\sqrt{3}/2)a'$, $a_y = a'$, $t_x = -\frac{3}{4}t$, and $t_y = -t$ for the hexagonal antidot lattice. This choice ensures that the lattice is commensurate with an antidot period. For the model of the square antidot lattice we symmetrically set $a_x = a_y = a'$ and $t_x = t_y = -t$. A magnetic field H is included in terms of a Peierls phase factor of the transfer integral. This rectangular lattice simulates the 2D system when we choose $t/E_F = \lambda_F/2\pi a'$, with $\lambda_F/a' \gg 1$, where λ_F is the Fermi wavelength.

Effects of scattering from impurities are introduced through the randomness of the site energy distributed uniformly with width W. In terms of the mean free path Λ in two dimensions, we have $W/E_F = (6\lambda_F^3/\pi^3 a'^2 \Lambda)^{1/2}$. Real antidot lattices have an inherent randomness arising from fabrication processes. In the following this disorder is introduced through fluctuations in antidot diameters distributed uniformly with width d_f around the mean value d.

The conductance of a finite antidot lattice is calculated in the framework of Landauer's formula[28]

$$G = \frac{2e^2}{h} \sum_{m,n} |t_{mn}|^2, \qquad (2.4)$$
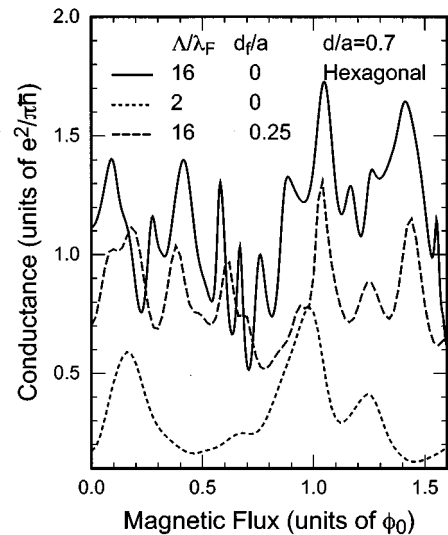

FIG. 2. Some examples of the magnetic-field dependence of the conductance of a hexagonal antidot lattice. Solid line: $d_f/a = 0$ and $\Lambda/\lambda_F = 16$ (nearly ballistic). Dotted line: $d_f/a = 0$ and $\Lambda/\lambda_F = 2$ (nearly diffusive). Dashed line: $d_f/a = 0.25$ and $\Lambda/\lambda_F = 16$ (antidot fluctuations).

where a factor 2 due to the spin degeneracy is included, and t_{mn} is the transmission amplitude at the Fermi energy from incoming state m to transmitted state n of the leads. The scattering matrix is calculated by use of the recursive Green's-function technique as described in a previous paper.[29] For systems with $L_x \sim L_y \gg \Lambda \gg a$, the average conductance is expected to provide information about an infinitely large antidot lattice in which the phase coherence length is of the order of L_x or L_y.

Figure 1 schematically illustrates the system for which actual numerical calculations are performed. The system has size $L_x/\lambda_F = 18$ and $L_y/\lambda_F = 20$ in the hexagonal case (a), $L_x/\lambda_F = L_y/\lambda_F = 20$ in the square case (b), and $L_x/\lambda_F = L_y/\lambda_F = 22$ in the square case (c) in which the primitive translation vector is 45° tilted from the x direction. The antidot period is chosen as $a = 4\lambda_F$, roughly following the parameters in actual antidot lattices used in experiments ($a \sim 200$ nm for $\lambda_F \sim 500$ Å).[10–12] In the following calculation we use $\beta = 1$ or 2, and $d/a = 0.7$ or 0.6, for which the number of 1D subbands below the Fermi level is two in the channel region between the nearest-neighbor antidots. Further, we choose $\lambda_F/a' = 7$. We perform calculations for more than 1000 samples typically to obtain the average.

III. NUMERICAL RESULTS

A. Hexagonal lattice

Figure 2 shows some examples of the calculated conductance as a function of the magnetic flux passing through the unit cell in the case that $\beta = 1$ and $d/a = 0.7$ corresponding to $U_0(\mathbf{R})/E_F = 4.38$. Three different cases have been chosen: (i) $d_f/a = 0$ and $\Lambda/\lambda_F = 16$ (nearly ballistic), (ii) $d_f/a = 0$ and $\Lambda/\lambda_F = 2$ (nearly diffusive), and (iii) $d_f/a = 0.25$ and $\lambda/\Lambda_F = 16$ (antidot fluctuations). The conductance exhibits an irregular oscillation which is similar to universal conductance fluctuations in the nearly diffusive case (ii), but seems to be more irregular for cases (i) and (iii). There seem to be some differences in the amplitude of fluctuations for varying magnetic field in these three cases, as will be discussed below.

Figure 3 gives the conductance averaged over more than 1000 different samples in the nearly ballistic regime $\Lambda/\lambda_F = 16$. In the absence of disorder in the antidot potential, the conductance exhibits an irregular oscillation even after the average. Both the phase and form of this oscillation vary sensitively depending on parameters like d/a, a/λ_F, and β, but are independent of the system size L_x and L_y. The oscillation will be shown below to correspond well to an AB oscillation of a single ideal ring, and therefore will be called an AB-type oscillation in the following.

With the increase of antidot fluctuations d_f, the amplitude of the irregular AB-type oscillation decreases. The AAS oscillation characterized by the period $\phi_0/2$ becomes dominant for fluctuations as large as $d_f/a = 0.25$, and its amplitude remains almost the same with a further increase in fluctuations. The amplitude of the oscillation is as large as $\Delta G \sim 0.3 e^2/h$. The AAS oscillation is accompanied by a weak negative magnetoresistance, i.e., a slight increase in the conductance as a function of a magnetic field except for the presence of the AAS oscillation.
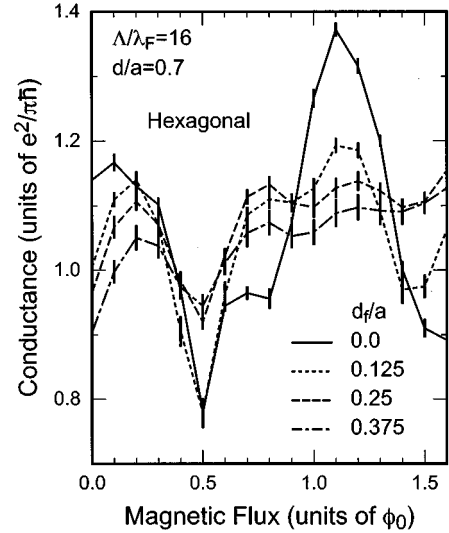

FIG. 3. Conductance of a hexagonal antidot lattice as a function of magnetic flux ϕ passing through a unit cell for different values of the fluctuation of the antidot diameter d_f. The fluctuation $d_f/a = 0.25$ corresponds to the change by ± 1 of channel number through a narrowest path between the nearest-neighbor antidots. $\beta = 1$, $d/a = 0.7$, $L_x/\lambda_F = 18$, and $L_y/\lambda_F = 20$.

The AAS oscillation is essentially independent of the detail in the spatial variation of the antidot potential, as shown in Fig. 4, where the conductance for the steepness parameter $\beta = 2$ is compared with that for $\beta = 1$ in the cases $d_f/a = 0.25$ and $\Lambda/\lambda_F = 16$. A slight difference in the absolute value of the conductance comes from the difference in the effective channel width between nearest antidots. In fact, although the classical channel width for electrons having Fermi energy is the same, it becomes effectively larger for electrons having a lower energy for $\beta = 2$ than those for $\beta = 1$. Quantum mechanically, the energy of 1D subbands below the Fermi level is lower for $\beta = 2$ than for $\beta = 1$, leading to an enhancement of the velocity along the channel for $\beta = 2$.
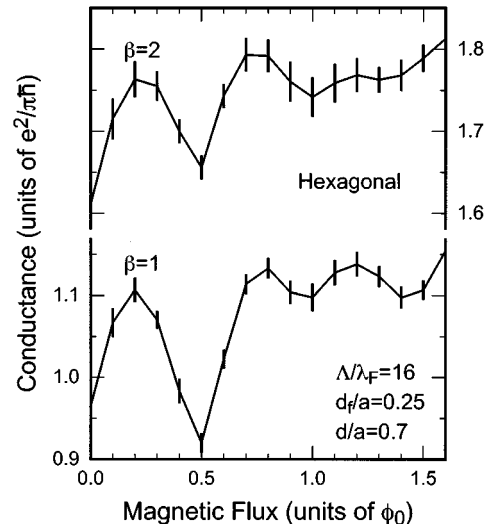

FIG. 4. The dependence on the steepness of the antidot potential for the hexagonal lattice with $d_f/a = 0.25$ and $\Lambda = \lambda_F = 16$.
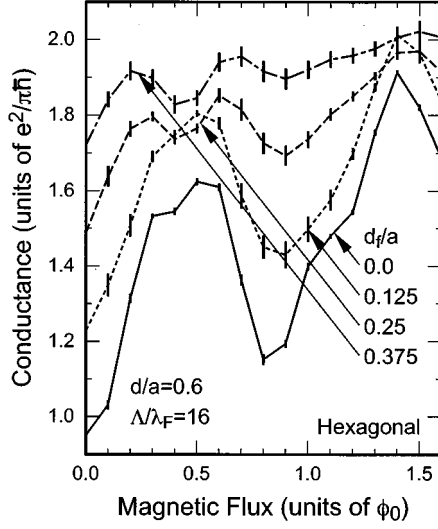
FIG. 5. Calculated conductance of a hexagonal lattice for $d/a=0.6$, $\beta=1$, and $\Lambda/\lambda_F=16$.

Figure 5 shows the conductance for antidots with a smaller mean diameter $d/a=0.6$. The other parameters are the same as those for Fig. 3. The irregular AB-type oscillation is again dominant in the absence of fluctuations in the antidot potential ($d_f/a=0$). Note that the form of the oscillation for $d_f/a=0$ is completely different from that shown in Fig. 3. In fact, the conductance takes a local maximum near $\phi/\phi_0=0$ in Fig. 3, while it takes a minimum in Fig. 5. With an increase in the fluctuation of the antidot potential, this irregular oscillation is again taken over by the more regular AAS oscillation. The AAS oscillation is dominant for $d_f/a=0.25$, but the dip at $\phi/\phi_0=\frac{3}{2}$ has become invisibly small. Further, the dip position is slightly shifted to the lower magnetic-field side. This can be understood as a result of the reduction in the ratio between the effective radius of the typical electron pass circling an antidot and the effective channel width.

It should be noted that the contribution of the irregular AB-type oscillation diminishes with the decrease in the mean free path Λ even in the absence of disorder in the antidot potential. In fact, a beautiful AAS oscillation manifests itself in the diffusive regime where $\Lambda/\lambda_F=2$ or $\Lambda/a=1/2$.[19] This corresponds to the AAS oscillation observed in metallic diffusive rings.[15,16]

B. Square lattice

Figure 6 shows some examples of calculated conductance of a square antidot lattice [Fig. 1(b)] as a function of the magnetic flux passing through the unit cell in the case when $\beta=1$ and $d/a=0.7$, corresponding to $U_0(\mathbf{R})/E_F=4.85$. The conductance exhibits an irregular oscillation similar to universal conductance fluctuations.

This irregular AB-type oscillation disappears, and is eventually taken over by an AAS oscillation with an increase in the disorder in the antidot potential. The critical amplitude of the fluctuation in the antidot diameter is about the same as that in the hexagonal lattice.[19]

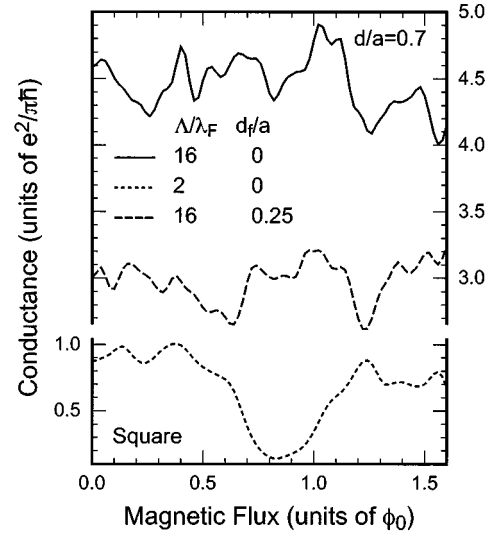Figure 7 compares the conductance of the square antidot

FIG. 6. Some examples of the magnetic-field dependence of the conductance of a square antidot lattice. Solid line: $d_f/a=0$ and $\Lambda/\lambda_F=16$ (nearly ballistic). Dotted line: $d_f/a=0$ and $\Lambda/\lambda_F=2$ (nearly diffusive). Dashed line: $d_f/a=0.25$ and $\Lambda/\lambda_F=16$ (antidot fluctuations).

lattice where the crystal axis is at an incline of 45° against the direction of the current [Fig. 1(c)] with that of the parallel square lattice in the presence of strong disorder in the antidot potential. The system size ($L_x/\lambda_F=L_y/\lambda_F=22$) is similar to that of other systems and the other parameters are the same as in Fig. 3. The conductance is slightly smaller than that of the parallel square lattice. This is presumably due to the fact that the reflection probability in the first and second rows of antidots is larger, and is certainly not a bulk effect. The large statistical errors make it impossible to see the AAS oscillation.

There are notable differences between the results in the square lattice and those in the hexagonal lattice. The follow-
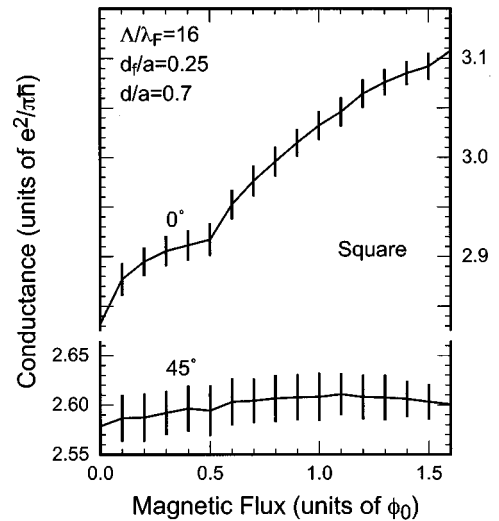

FIG. 7. Conductance of an inclined square lattice. The angles between the direction of the current and crystal axis are denoted in the figure. $L_x/\lambda_F=L_y/\lambda_F=22$ for 45°. $L_x/\lambda_F=L_y/\lambda_F=20$ for 0°.
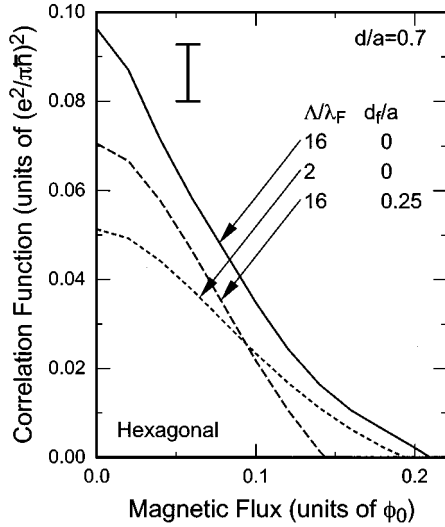
FIG. 8. Calculated correlation function of the conductance in a hexagonal lattice with $d/a = 0.7$. The solid, dotted, and dashed lines correspond to cases of (i) nearly ballistic, (ii) nearly diffusive, and (iii) antidot fluctuations. The vertical bar represents typical statistical errors.

FIG. 9. Calculated correlation function of the conductance in a square lattice with $d/a = 0.7$.

ing are some examples of the features of the square lattice in comparison with those of the hexagonal lattice.

(1) The absolute value of the conductance is much larger.

(2) The irregular oscillation in the absence of the disorder in the antidot potential has a smaller amplitude.

(3) The AAS oscillation in the presence of strong disorder in the antidot potential is much weaker.

C. Fluctuations

In order to see the features of the magnetic fingerprint in antidot lattices, we shall calculate the correlation function defined by

$$F(\Delta B) = \langle \langle [g(B + \Delta B) - \langle g(B + \Delta B) \rangle_B][g(B)$$
$$- \langle g(B) \rangle_B] \rangle_B \rangle_S , \qquad (3.1)$$

where $\langle \ \rangle_B$ is the average of the conductance of a single sample over the magnetic flux in the range $0.1 < \phi/\phi_0 < 1.7$, and $\langle \ \rangle_S$ means the sample average. Figures 8 and 9 show results for the hexagonal and square lattices, respectively. The correlation field is given by $\phi/\phi_0 \sim 0.1$ for both hexagonal and square lattices, almost independent of the strength of impurity scattering and the disorder in the antidot potential. This field corresponds roughly to a single flux quantum in the total area of the system, in agreement with the case of universal conductance fluctuations in diffusive systems.[30,31]

The amount of conductance fluctuations as a function of the magnetic field becomes smaller in the presence of randomness, due either to impurities or antidot disorder. On the other hand, fluctuations of the conductance among different samples in a fixed magnetic field are close to the universal value $\Delta G \sim 0.3 e^2/\pi \hbar$ irrespective of systems, which corresponds to the universal value of the fluctuations in the two-dimensional system in magnetic fields.[30,31] This means that fluctuations for varying magnetic fields can be considerably
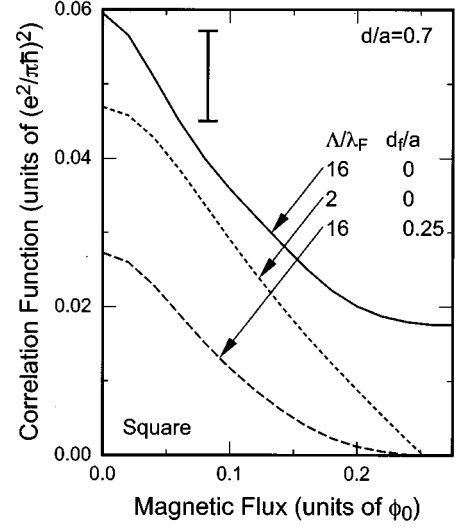
smaller than fluctuations among different samples, in contrast to the case of the universal conductance fluctuations.

IV. DISCUSSION AND CONCLUSION

An irregular AB-type oscillation appears in the near-ballistic antidot lattice, particularly in the hexagonal case. A close examination of the dependence on parameters such as d/a shows that the characteristic feature of the oscillation varies systematically as a function of d/a. In fact, in certain narrow regions of d/a the conductance has a local maximum at $\phi = 0$, and in other regions it has a local minimum. This is a result of the interference of electron waves in a single ballistic AB ring. In particular, the strong dependence on d/a is due to the interference of waves associated with the highest 1D subband occupied by electrons in the channel region between two adjacent antidots, because their 1D wave vector is quite sensitive to the change in the parameters.

Let us consider, for example, a ballistic AB ring with radius $a/2$ shown in Fig. 10. The potential in each region divided by the dashed lines are chosen as

$$v(\mathbf{r}) = \begin{cases} v_0(\mathbf{r}) & (\text{I: } y < x < \sqrt{3}, \quad y < -\sqrt{3}x + a) \\ v_{\mathbf{a}_1}(\mathbf{r}) & (\text{II: } y < x/\sqrt{3}, \quad y > -\sqrt{3}x + a) \\ v_{\text{wire}}(|\mathbf{r}|) & (\text{III: } y > x/\sqrt{3}, \quad |\mathbf{r}| < a), \end{cases} \qquad (4.1)$$

where the origin is chosen at the center of the ring, $v_{\mathbf{R}}(\mathbf{r})$ is defined in Eq. (2.1), $u_0 = U_0(\mathbf{0}) = U_0(\mathbf{a}_1)$, and

$$v_{\text{wire}}(y) = u_0 \left| \cos\left(\frac{\pi y}{a}\right) \cos^2\left(\frac{\pi y}{2a}\right) \right|^{4\beta/3} . \qquad (4.2)$$

The potential in the other region is chosen in a symmetric way. The system is connected at $x = \pm \sqrt{3}/2a$ to infinite wires or leads whose potential is given by $v_{\text{wire}}(y)$. Further, the system and leads are confined by an abrupt and infinite barrier at the position satisfying $v(y) = 2E_F$.
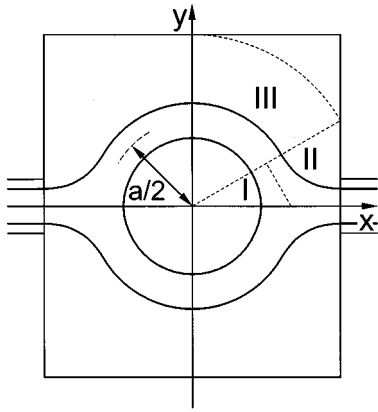
FIG. 10. A schematic illustration of a single AB ring. The ring with radius $a/2$ is connected to an ideal lead at $x = \pm \sqrt{3}/2a$.

FIG. 11. Two typical types of conductance across a single ring in a two-terminal geometry. $a/\lambda_F = 8$.

The conductance G is given by the probability for electron waves incident from the left lead transmitted to the right lead according to Landauer's formula.[28] The Onsager relation requires that G in such a two-terminal geometry is an even function of the magnetic field, and leads to the expansion[18]

$$G(\phi) = G_0 + G_1 \cos(2\pi\phi/\phi_0) + G_2 \cos(4\pi\phi/\phi_0) + \cdots. \tag{4.3}$$

Waves rotating around the ring many times, and reflected back and forth at the junctions with the leads, make complicated interferences. The coefficient G_1 is expected to become negative when the interference is constructive at the junction with the lead on the right hand side in the absence of a flux, i.e., $kL = n\pi$, with n an integer, where k is the wave vector in the absence of a magnetic field and $2L$ is the circumference of the ring. On the other hand, G_1 becomes positive when the interference in the absence of a field is destructive, i.e., $kL = (n + 1/2)\pi$. This is analogous to the well-known Fabry-Perot interference.

Figure 11 shows the typical conductance of an AB ring in the case when the current is carried by a single 1D channel. The parameters characterizing the ring are chosen in such a way that the diameter of the ring and the effective width of the wire are close to those for the highest 1D channel in the hexagonal antidot lattice ($a/\lambda_F = 4$ and $d/a = 0.7$). Apart from a sharp dip near $\phi/\phi_0 = \frac{1}{2}, \frac{3}{2}, \ldots$, arising from the symmetry of the wave function in the ring,[18,32] the results show the change between two rigid phases corresponding to the change in the signature of G_1. The sharp dip at half-integer values of ϕ/ϕ_0 disappears in multichannel cases.

The absolute value of the conductance is much smaller in the hexagonal lattice than in the square lattice. This can be understood in the classical trajectory model, which predicts that electrons perform much more complicated motion and stay much longer in the hexagonal lattice than in the square lattice, as was demonstrated in a simple model.[12] This is presumably the main origin of the enhancement of the AAS oscillation in the hexagonal lattice. In the square lattice a runaway trajectory moving along a crystal axis is known to make a dominant contribution to the conductivity.[33] This is
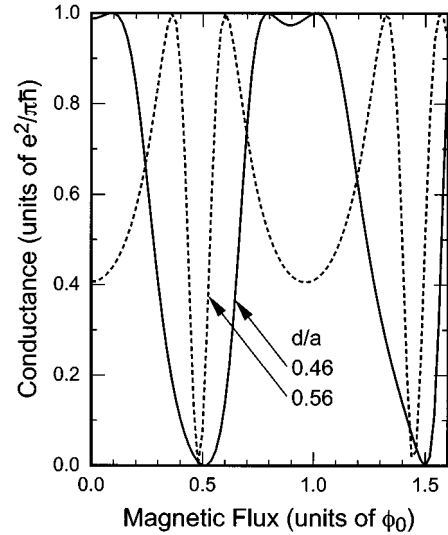
known to be the case even in square lattices with a small period.[7] Presumably such a trajectory plays less important roles in hexagonal lattices with a small period.

The essential features of the AAS oscillation observed experimentally[10-12] can be summarized as follows.

(1) The oscillations are observed clearly in hexagonal lattices, but are almost invisible in square lattices.[11,12]

(2) The amplitude of the oscillations extrapolated up to absolute zero temperature is $\Delta\sigma \sim 0.3 e^2/h$ in hexagonal lattices.

(3) The negative magnetoresistance is observed together with the AAS oscillation.

(4) The amplitude of the oscillations normalized by the zero-field resistance is larger than that observed in diffusive metallic rings.[14,15]

These features, particularly (1)–(3), can be explained quite well by the present calculation if we assume the presence of sizable amount of disorder in the antidot potential itself. The difference between the antidot lattices and metallic rings (4) can be understood by a large difference in the absolute value of the resistivity itself.

The amount of fluctuations in the antidot diameter, $d_f/a \gtrsim 0.25$, necessary for the clear AAS oscillation, may seem to be larger than fluctuations present in antidot lattices used in experiments. This is not necessarily true, however. In actual antidot lattices various kinds of fluctuations are possible, such as those in the shape and position of each antidot. Remote ionized donors giving two-dimensional electrons themselves are known to cause potential fluctuations,[34] which may also be regarded as fluctuations in the antidot potential. In the present calculation, all kinds of long-range potential fluctuations have been replaced by a single kind of disorder, i.e., by the fluctuation d_f of the antidot diameter.

It is well known that the lowest-order quantum correction to the Boltzmann conductivity is of the order of e^2/h in diffusive two-dimensional systems. In a conductor with a hollow geometry, this quantum correction is modified by the magnetic flux passing through the hollow region, leading to

the AAS oscillation.[9] In diffusive systems the mean free path is much less than the typical system dimension, and effects of the reflection by the boundary are negligible. In the antidot lattice, reflection or scattering by the antidot potential is essential, and both AAS oscillation and weak-localization effects are the consequence of the randomness in the antidot potential.

In conclusion, we have calculated the conductance of antidot lattices in weak magnetic fields, using a recursive Green's-function technique. An AAS oscillation becomes visible either when an appreciable amount of fluctuations $d_f/a \gtrsim 0.25$ is introduced in the antidot potential, or when the mean free path becomes less than the antidot period. The amplitude of the AAS oscillation is much larger in hexagonal lattices than in square lattices, in excellent agreement with experiments.

[1] D. Weiss, M. L. Roukes, A. Menschig, P. Grambow, K. von Klitzing, and G. Weimann, Phys. Rev. Lett. **66**, 2790 (1991).

[2] A. Lorke, J. P. Kotthaus, and K. Ploog, Phys. Rev. B **44**, 3447 (1991); Superlatt. Microstruct. **9**, 103 (1991).

[3] T. Yamashiro, J. Takahara, Y. Takagaki, K. Gamo, S. Namba, S. Takaoka, and K. Murase, Solid State Commun. **79**, 885 (1991).

[4] R. Fleischmann, T. Geisel, and R. Ketzmerick, Phys. Rev. Lett. **68**, 1367 (1992).

[5] D. Weiss, K. Richter, A. Mensching, R. Bergmann, H. Schweizer, K. von Klitzing, and G. Weimann, Phys. Rev. Lett. **70**, 4118 (1993).

[6] D. Weiss, K. Richter, E. Vasiliadou, and G. Lütjering, Surf. Sci. **305**, 408 (1994).

[7] S. Ishizaka, F. Nihey, K. Nakamura, J. Sone, and T. Ando, Phys. Rev. B **51**, 9881 (1995).

[8] S. Uryu and T. Ando, Jpn. J. Appl. Phys. **34**, 4295 (1995).

[9] B. L. Al'tshuler, A. G. Aronov, and B. Z. Spivak, Pis'ma Zh. Éksp. Teor. Fiz. [JETP Lett. **33**, 94 (1981)] **33**, 101 (1981).

[10] G. M. Gusev, Z. D. Kvon, L. V. Litvi, Yu. V. Astaushev, A. K. Kalagin, and A. I. Toropov, Pis'ma Zh. Éksp. Teor. Fiz. **55**, 129 (1991) [JETP Lett. **55**, 123 (1992)].

[11] K. Nakamura, S. Ishizaka, and F. Nihey, Physica B **197**, 144 (1994).

[12] F. Nihey, S. W. Hwang, and K. Nakamura, Phys. Rev. B **51**, 4649 (1995).

[13] Y. Aharonov and D. Bohm, Phys. Rev. **115**, 485 (1959).

[14] D. Yu. Sharvin and Yu. V. Sharvin, Pis'ma Zh. Éksp. Teor. Fiz. **34**, 285 (1981) [JETP Lett. **34**, 272 (1981)].

[15] G. J. Dolan, J. C. Licini, and D. J. Bishop, Phys. Rev. Lett. **56**, 1493 (1986).

[16] B. Douçot and R. Rammal, Phys. Rev. Lett. **55**, 1148 (1985); J. Phys. (Paris) **47**, 973 (1986).

[17] A. Yacoby, R. Schuster, and M. Heiblum, Phys. Rev. B **53**, 9583 (1996).

[18] Y. Gefen, Y. Imry, and M. Ya. Azbel, Phys. Rev. Lett. **52**, 129 (1984); Surf. Sci. **142**, 203 (1984).

[19] T. Nakanishi and T. Ando, Physica B (to be published).

[20] G. Kirczenow, Surf. Sci. **263**, 330 (1992).

[21] G. Kirczenow, Phys. Rev. B **46**, 1439 (1992).

[22] B. L. Johnson and G. Korczenow, Phys. Rev. Lett. **69**, 672 (1992).

[23] B. L. Johnson, C. Barnes, and G. Kirczenow, Phys. Rev. B **46**, 15 302 (1992).

[24] S. Ishizaka, K. Nakamura, and T. Ando, Phys. Rev. B **48**, 12 053 (1993).

[25] H. Xu, Phys. Rev. B **50**, 8469 (1994); **50**, 12 254 (1994).

[26] H. Silberbauer and U. Rössler, Phys. Rev. B **50**, 11 911 (1994).

[27] I. V. Zozulenko, F. A. Maaø, and E. H. Hauge, Phys. Rev. B **51**, 7058 (1995).

[28] R. Landauer, IBM J. Res. Dev. **1**, 223 (1957); Philos. Mag. **21**, 863 (1970).

[29] T. Ando, Phys. Rev. B **44**, 8017 (1991).

[30] P. A. Lee and A. D. Stone, Phys. Rev. Lett. **55**, 1622 (1985).

[31] A. D. Stone, Phys. Rev. Lett. **56**, 2692 (1985).

[32] S. Datta and S. Bandyopadhyay, Phys. Rev. Lett. **58**, 717 (1987).

[33] É. M. Baskin, G. M. Gusev, Z. D. Kvon, A. G. Pogosov, and M. V. Éntin, Pis'ma Zh. Éksp. Teor. Fiz. **55**, 649 (1992) [JETP Lett. **55**, 678 (1992)].

[34] J. A. Nixon and J. H. Davies, Phys. Rev. B **41**, 7929 (1990).